

Table S1.  $^1\text{H}$  and  $^{13}\text{C}$  chemical shift values of compound **13b** (see Figure 4 for corrole numbering)

Position	$\delta$ $^1\text{H}$ (ppm)	$\delta$ $^{13}\text{C}$ (ppm)
1, 4		122.73, 129.0*
2		131.55
3	8.76	120.44
5, 15		-
6, 14; 9, 11		140.13, 136.82, 139.95, 136.45*
7, 13	8.67-8.64	125.23
8, 12	8.65	122.87
10		105.97
16, 19		132.13, 126.86*
17	8.58	122.39
18	9.65	116.63
20		133.88
21		138.76
22	7.33	127.80
23		138.18
24	2.61	20.12
25	1.91	19.82
26		142.10
27	8.27	133.62
28	8.23	124.94
29		144.25

\* Chemical shift values may be interchanged.

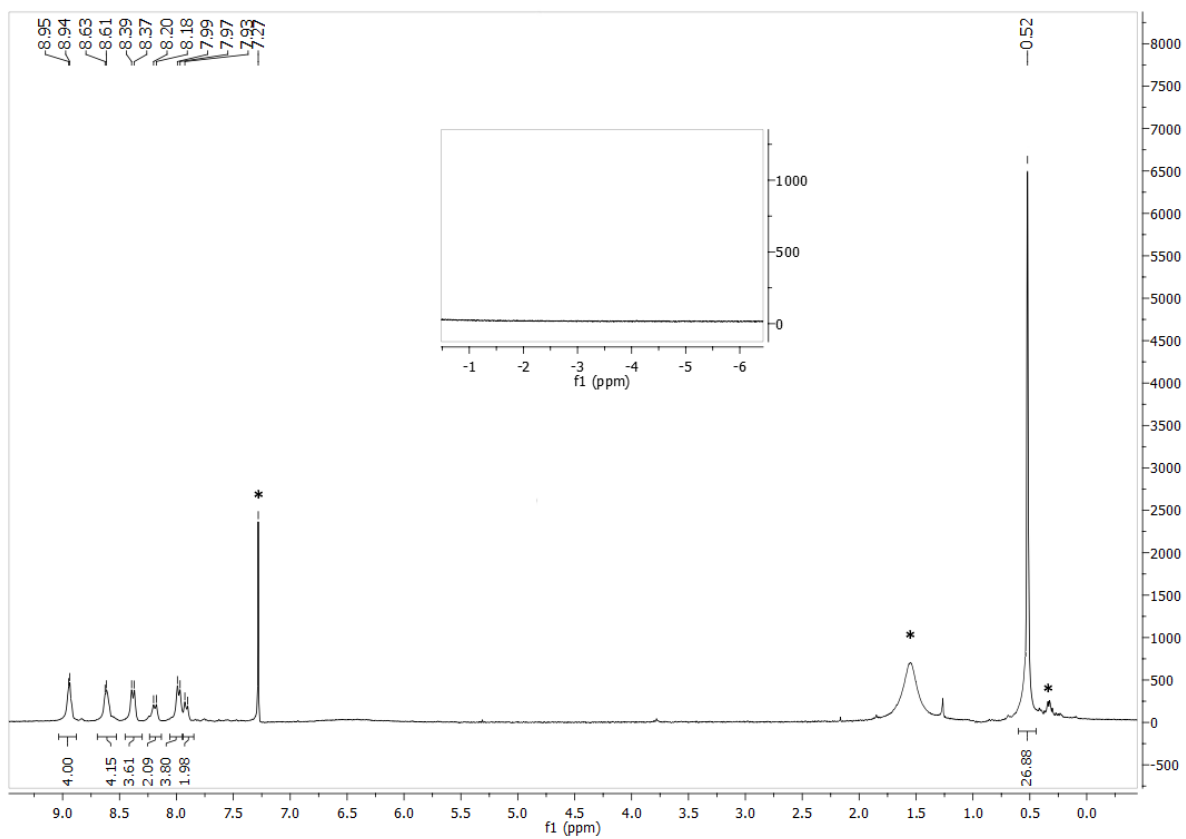


Figure S1:  $^1\text{H}$  NMR of **6** in  $\text{CDCl}_3$

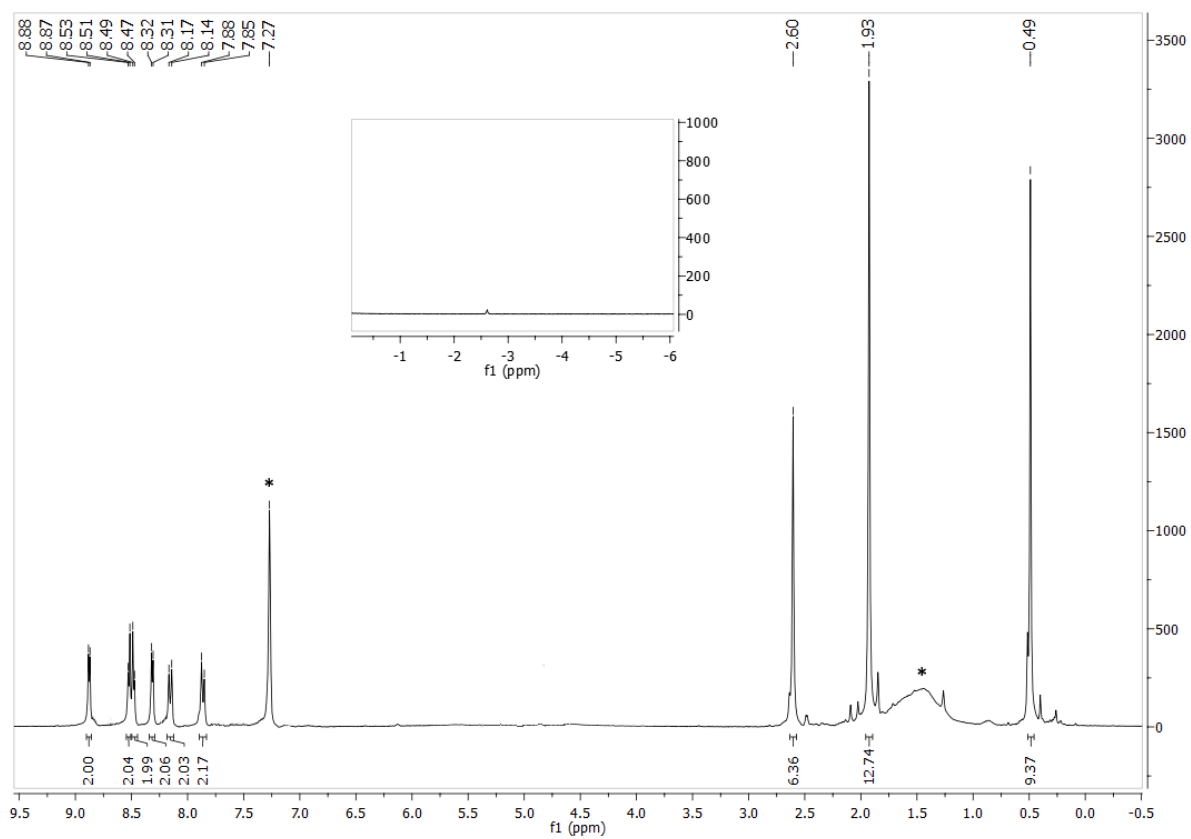


Figure S2:  $^1\text{H}$  NMR of **7** in  $\text{CDCl}_3$

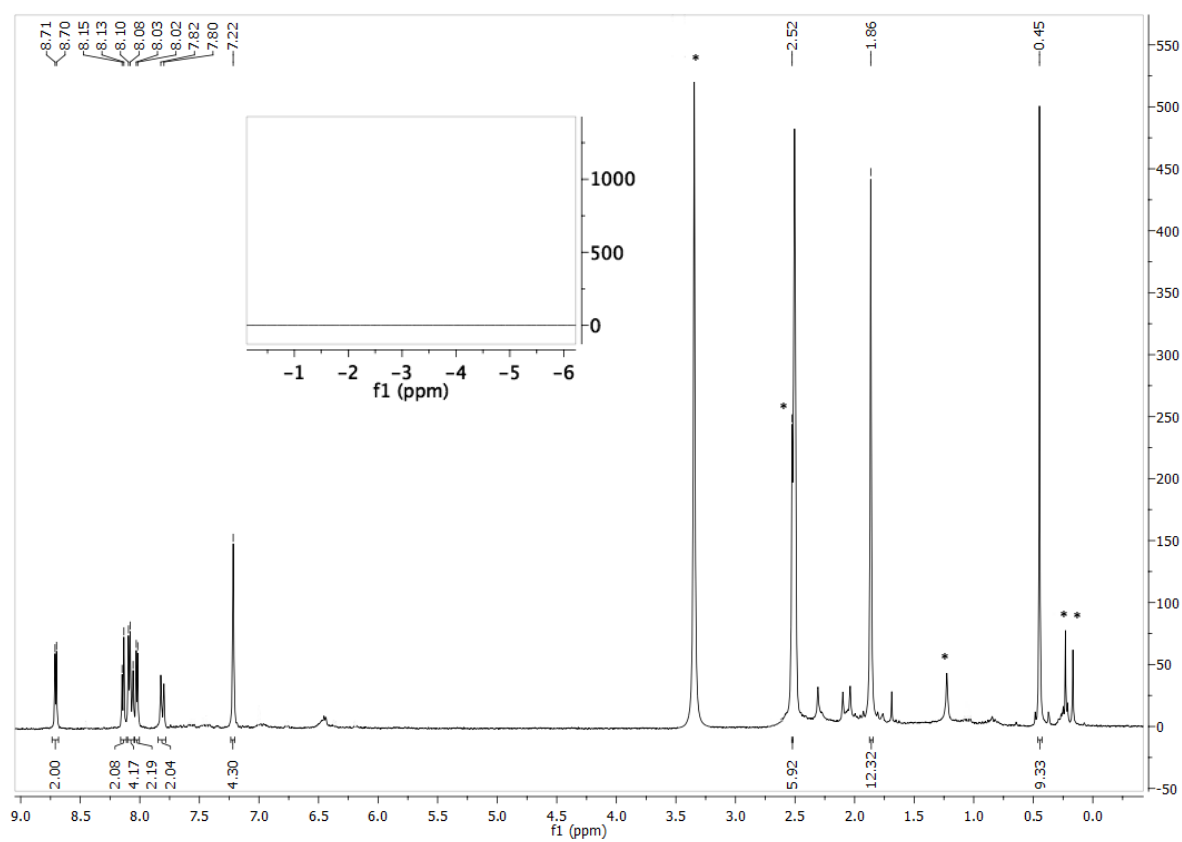


Figure S3:  $^1\text{H}$  NMR of **7** in  $\text{DMSO-d}_6$

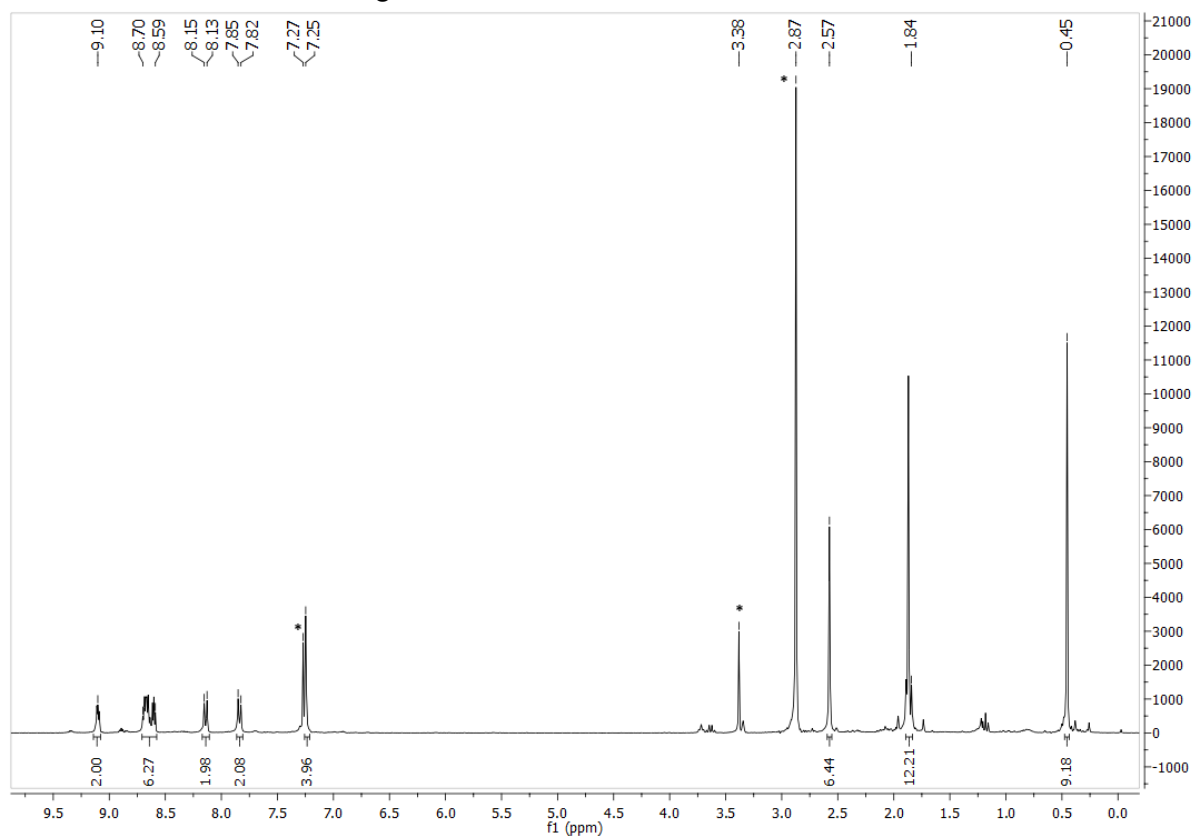


Figure S4:  $^1\text{H}$  NMR of **10b** in  $\text{CDCl}_3 + 50\ \mu\text{L}\ \text{CD}_3\text{OD}$  ("b" indicates phosphorus complex with two  $-\text{OCD}_3$  as axial ligands)

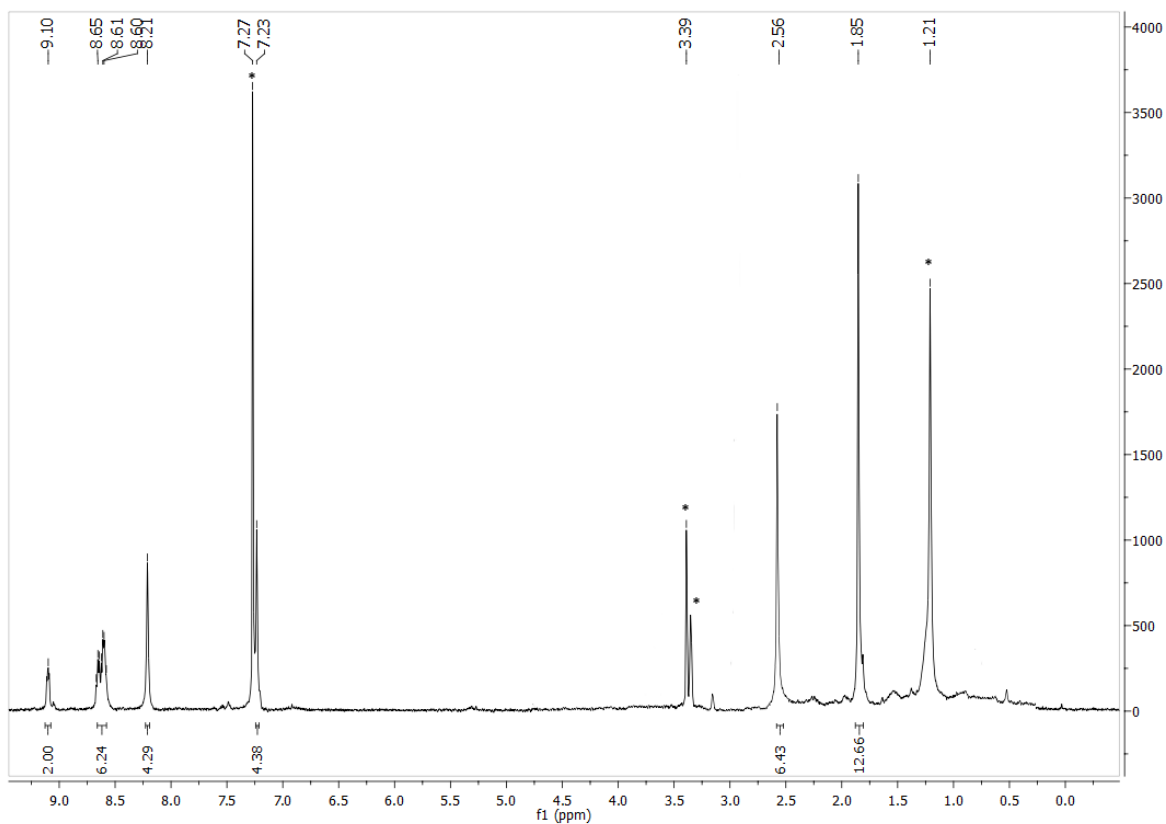


Figure S5:  $^1\text{H}$  NMR of **11** in  $\text{CDCl}_3 + 50\ \mu\text{L}$   $\text{CD}_3\text{OD}$  (“**b**” indicates phosphorus complex with two  $-\text{OCD}_3$  as axial ligands)

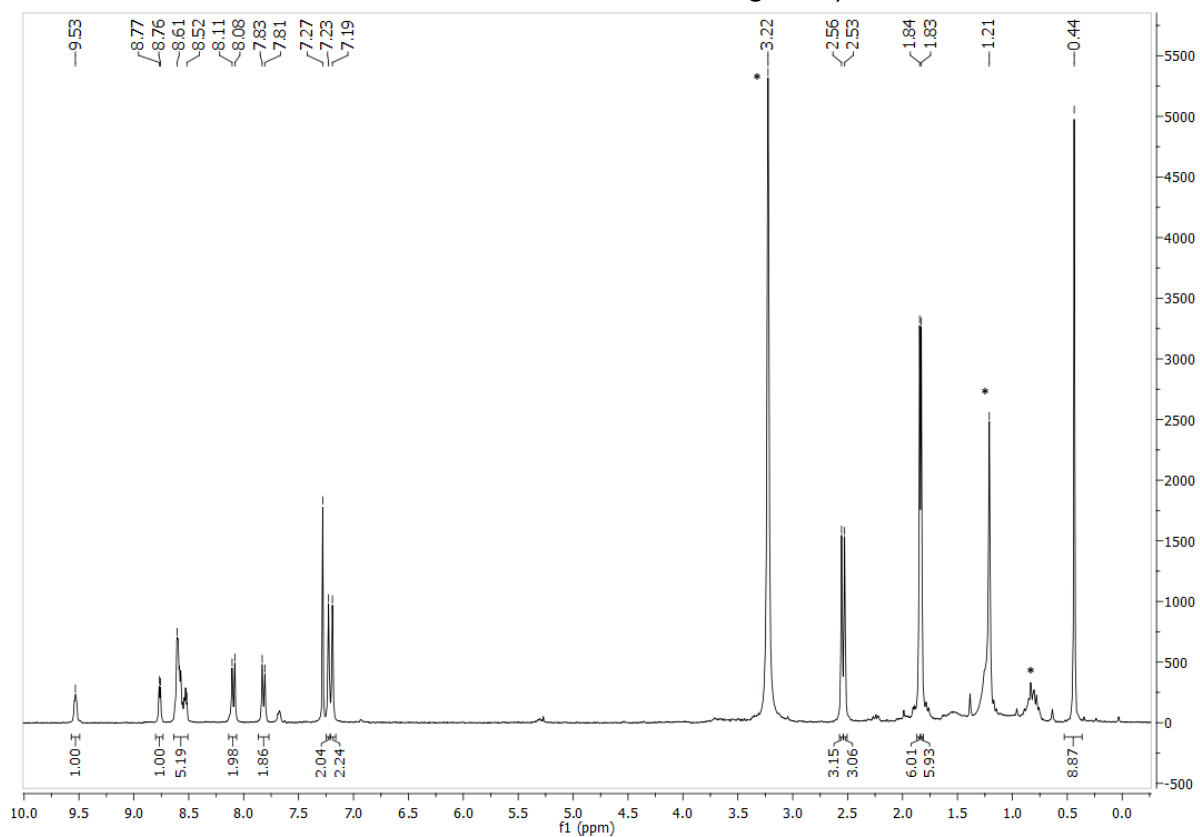


Figure S6:  $^1\text{H}$  NMR of **12** in  $\text{CDCl}_3 + 50\ \mu\text{L}$   $\text{CD}_3\text{OD}$  (“**b**” indicates phosphorus complex with two  $-\text{OCD}_3$  as axial ligands)

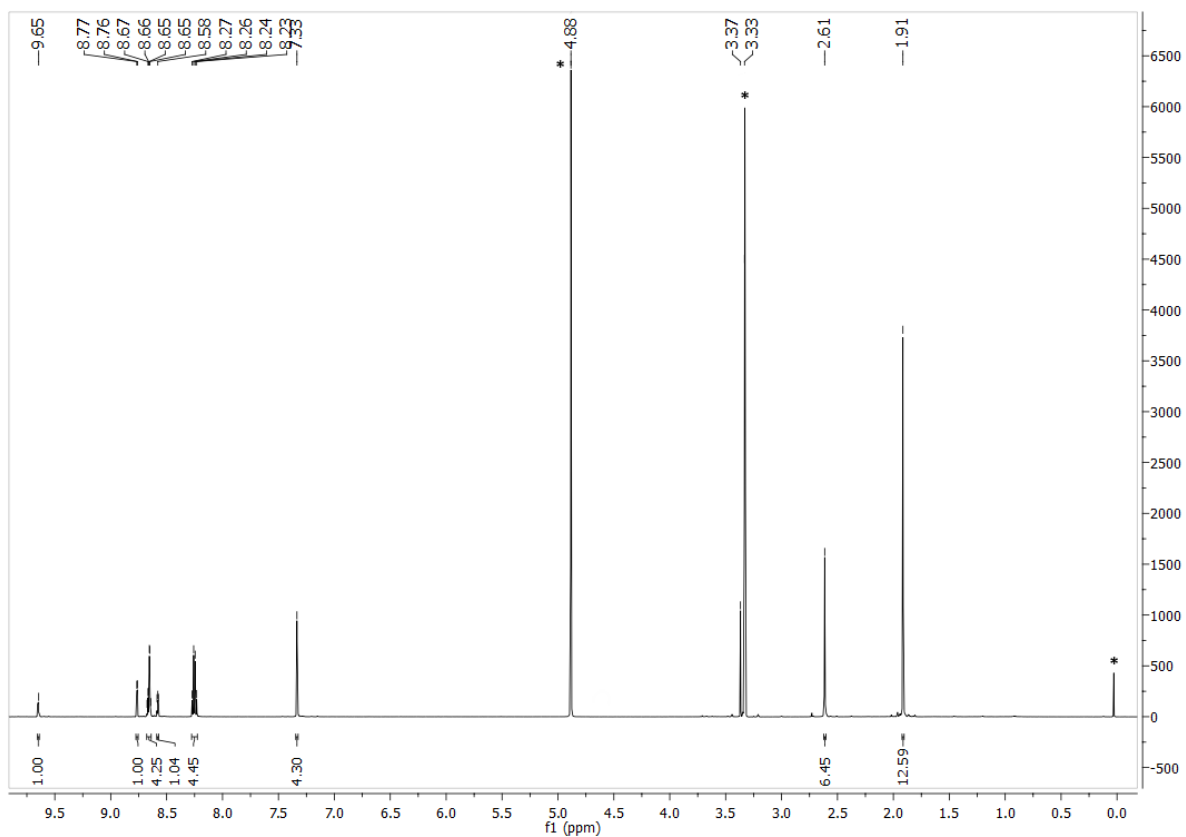


Figure S7:  $^1\text{H}$  NMR of **13b** in  $\text{CD}_3\text{OD}$

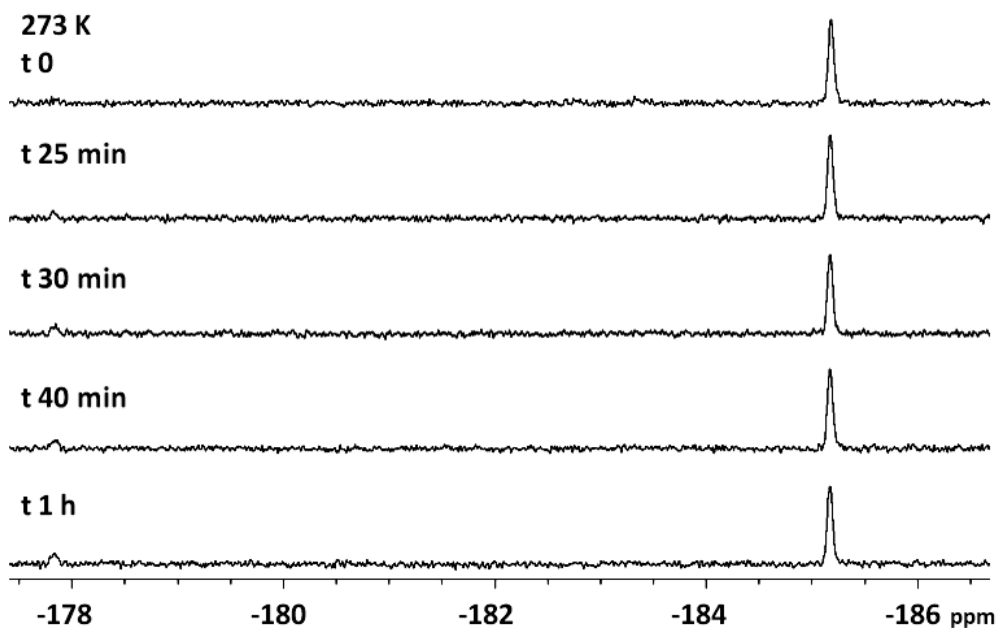


Fig. S8 Comparison between  $^{31}\text{P}$  NMR spectra of compound **13** recorded at different time in  $\text{CD}_3\text{OD}$  at 273 K.

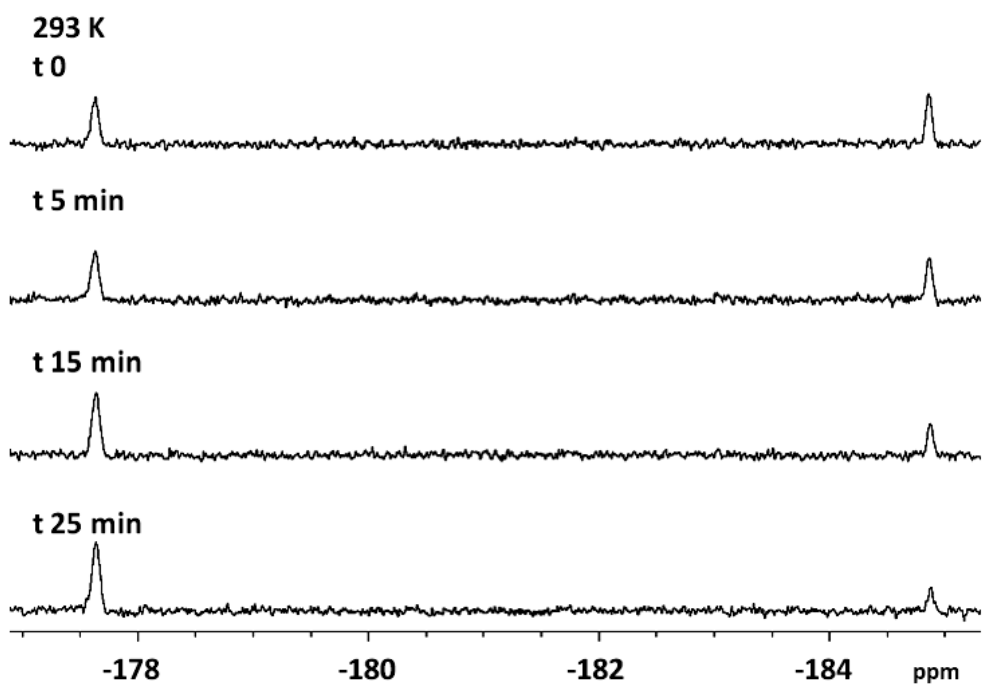


Fig. S9 Comparison between  $^{31}\text{P}$  NMR spectra of compound **13** recorded at different time in  $\text{CD}_3\text{OD}$  at 293 K.

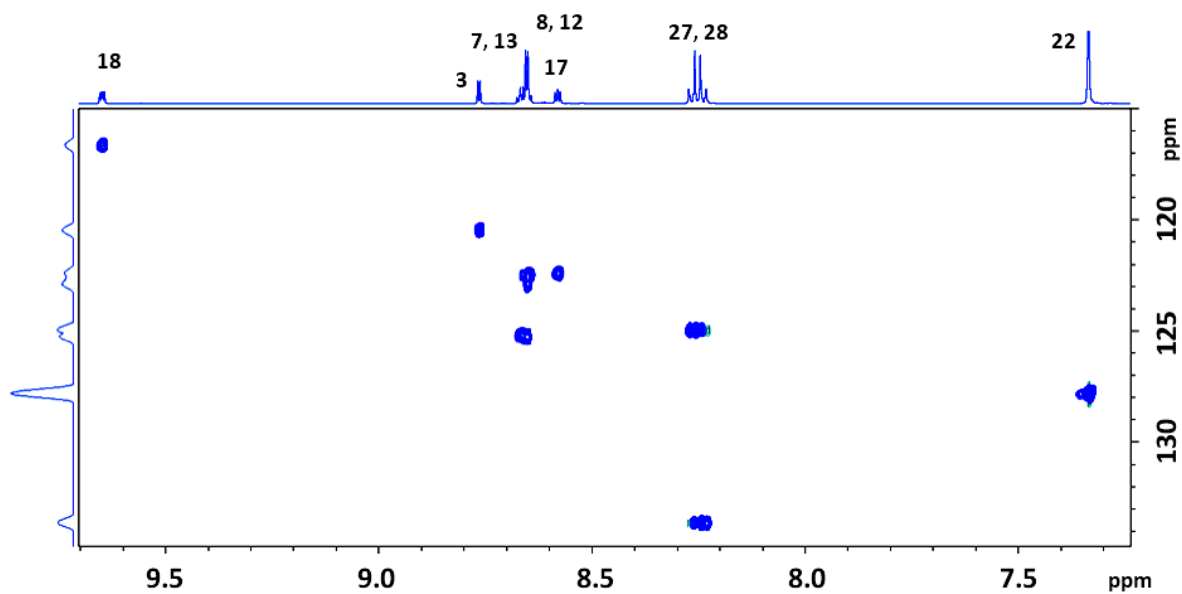


Fig. S10  $^1\text{H}$ - $^{13}\text{C}$  HSQC spectrum of compound **13b** in  $\text{CD}_3\text{OD}$  at 298 K.

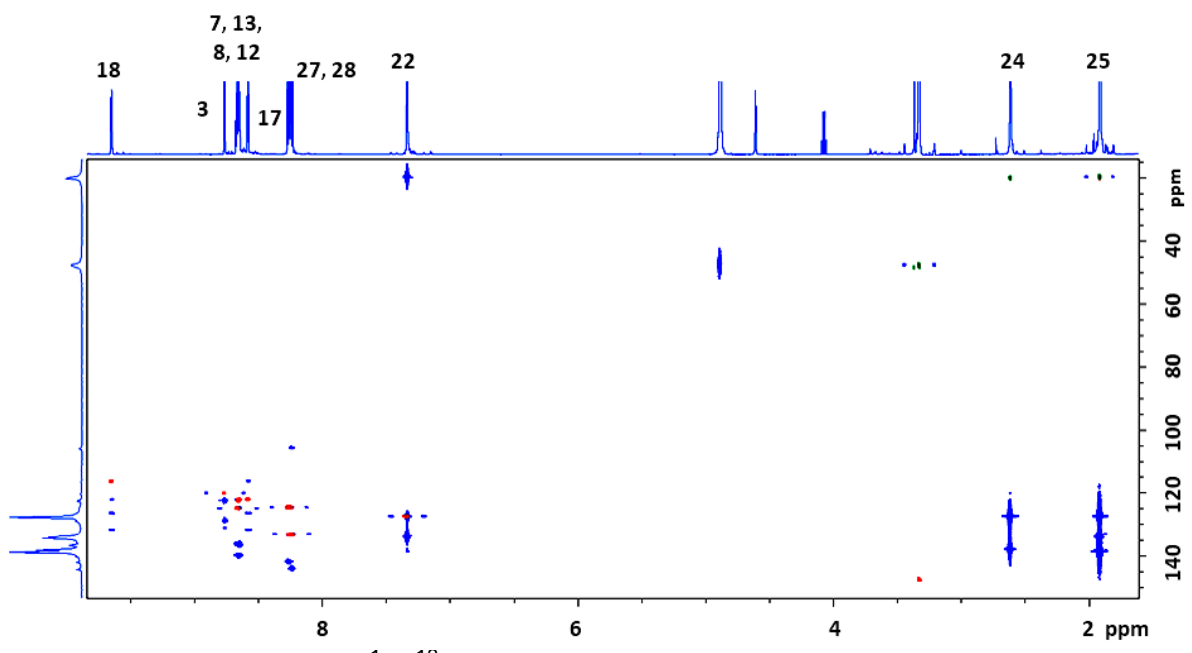


Fig. S11 Overlap between <sup>1</sup>H-<sup>13</sup>C HSQC (green aliphatic region; red aromatic region) and HMBC (blue) spectra of compound **13b** in CD<sub>3</sub>OD at 298 K.

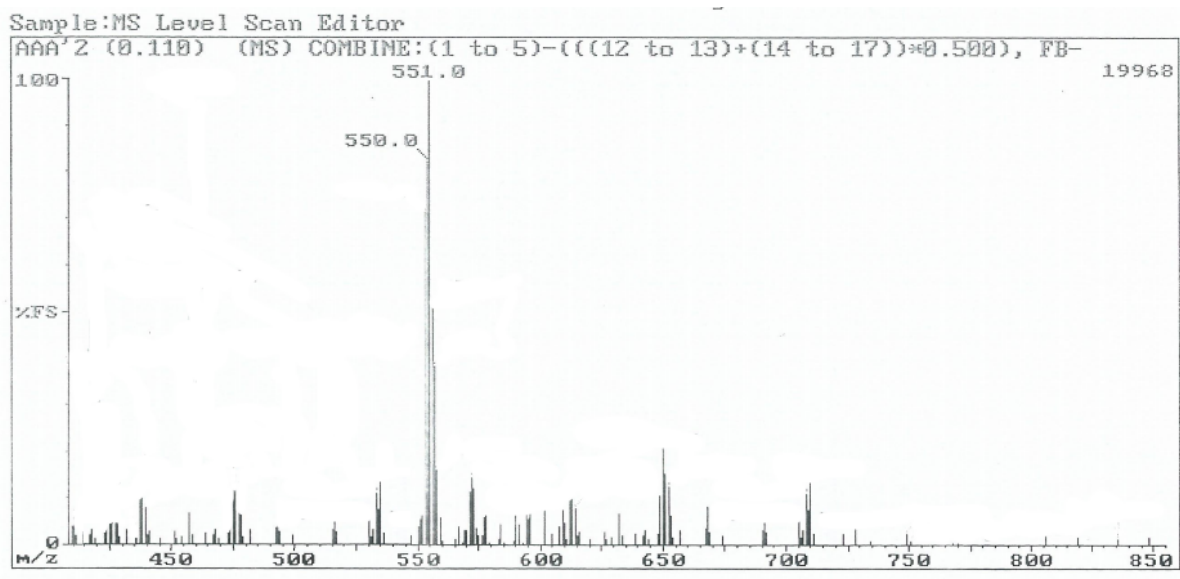


Figure S12: FAB MS<sup>-</sup> of **13** in CH<sub>3</sub>OH with *m*-nitrobenzyl alcohol(matrix)

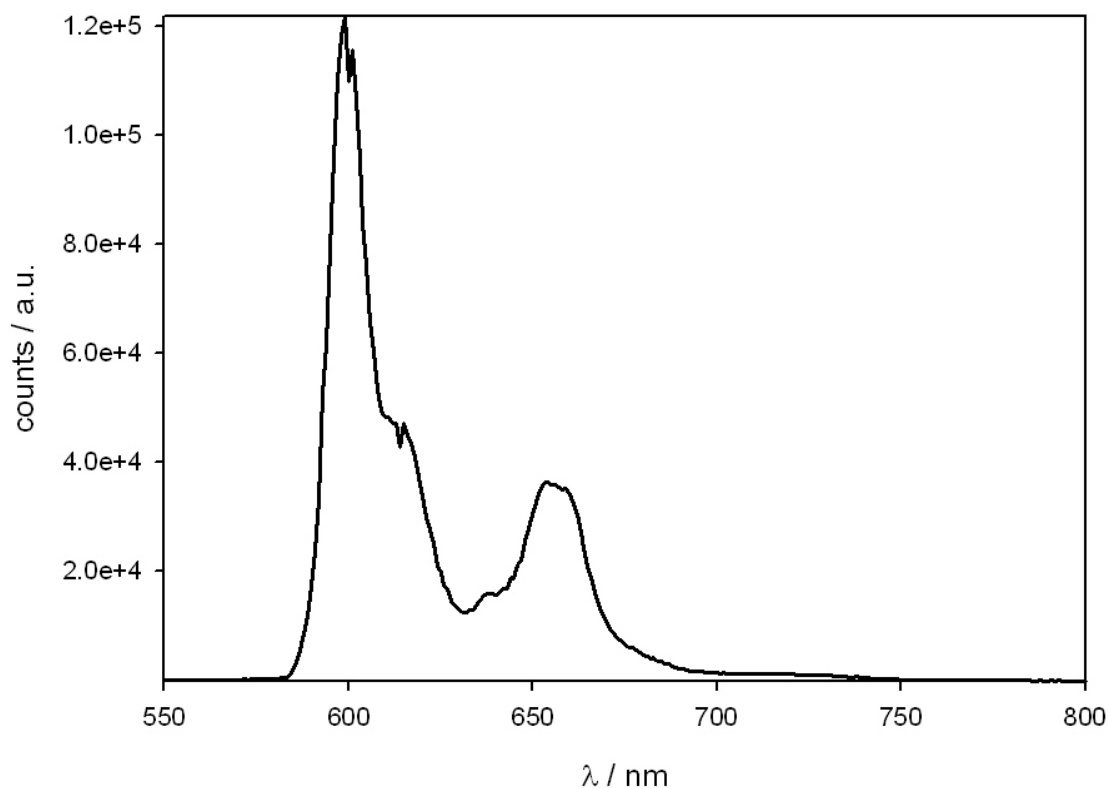
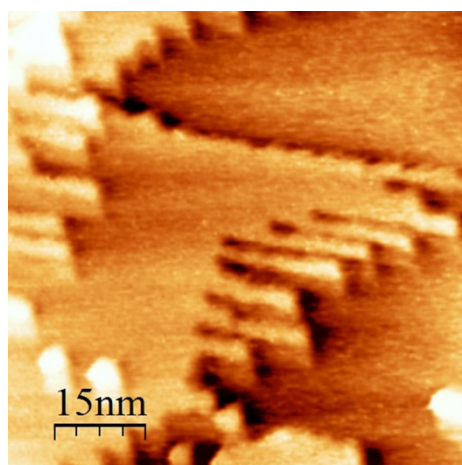


Figure S13 – Emission spectrum at  $T = 77\text{K}$  of **13b** in methanol ( $\lambda_{\text{exc}} = 410\text{ nm}$ ).

#### STM characterization of Au(111) surface after RGO deposition

The first evidence observed after the deposition was nano-fingers growth on the atomically flat Au (111) triangular steps (Figure S14).



**Figure S14.** STM images ( $I=1\text{ nA}$  and  $V=0.2\text{V}$ ) ( $150 \times 150\text{ nm}^2$ ) of Au(111) surface after RGO deposition. In the (a) and (b) panel two different regions that show the Nano-fingers formation.

Moreover the surface morphology undergoes strong modification during the STM scan as shown by successive recorded STM images reported in Figure S15. Previous results<sup>[1]</sup> have reported nanofinger formation on a clean gold surface. However Yin et.al. concluded that high-field conditions, i.e. Bias voltage of  $\sim 1.5\text{V}$  and tunneling currents of  $\sim 30\text{nA}$ - $50\text{nA}$  were required for the formation of Nano fingers via gold atom extraction from step edges, while under the low-field conditions, i.e. Bias voltage of



~0.1V and tunneling current of 5nA, the gold surface was not modified by repeated scanning at room temperature.<sup>[2]</sup> In our case, the formation of Nano fingers after the RGO deposition was readily observed, although we used a very low tunneling conditions (tunneling current of 1nA and bias potential of 0.2V). Our experimental evidences are in agreement with similar nano-fingers formation at low tunneling conditions reported by Wilson and co-workers, in the case of (S)-lysine onto the Au (111) surface.<sup>[3]</sup> Moreover the RGO-gold atom clusters appear very mobile on the surface also at room temperature without any further annealing at step edges and inside defect-free terraces and they are dynamic over time as shown by the successive recorded STM images in Figure S15. Similar behavior was reported in the case of insulin growth factor tripeptide adsorption.<sup>[4]</sup>

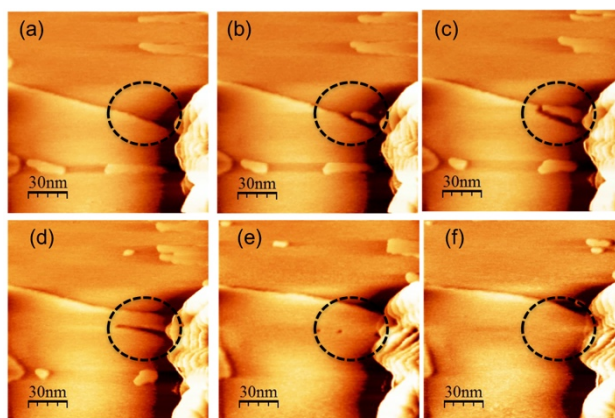


**Figure S15.** From (a) to (f) successive recorded STM images ( $I=1$  nA and  $V=0.2$ V) ( $150 \times 150 \text{ nm}^2$ ) of Au(111) surface after RGO deposition showing the progressive change in the finger growth caused by repeated scans of STM tip. The dotted circle denotes changes in the surface

- [1] F. Yin, *Phys. Rev. B.* **2006**, 73, 073405.
- [2] C. Schonenberger, J. A. M. Sondag-Huethorst, J. Jorritsma, L. G. J. Fokkink, *Langmuir* **1994**, 10, 611–614.
- [3] K. E. Wilson, H. A. Früchtl, F. Grillo, C. J. Baddeley, *Chem. Commun.* **2011**, 47, 10365-10367.
- [4] V. Humblot, A. Vallée, A. Naitabdi, F. Tielens, C.-M. Pradier, *J. Am. Chem. Soc.* **2012**, 134, 6579-6583.